Water Resources Research

RESEARCH ARTICLE
10.1029/2023WR036162

A Spatially-Distributed Machine Learning Approach for Fractional Snow Covered Area Estimation

Shalini Mahanthege[1], William Kleiber[2], Karl Rittger[3], Balaji Rajagopalan[4], Mary J. Brodzik[5], and Edward Bair[6]

[1]Department of Statistics, University of Missouri, Columbia, MO, USA, [2]Department of Applied Mathematics, University of Colorado at Boulder, Boulder, CO, USA, [3]Institute of Arctic and Alpine Research, University of Colorado at Boulder, Boulder, CO, USA, [4]Department of Civil, Environmental and Architectural Engineering, Cooperative Institute for Research in Environmental Sciences, University of Colorado, Boulder, CO, USA, [5]National Snow and Ice Data Center, Cooperative Institute for Research in Environmental Sciences, University of Colorado, Boulder, CO, USA, [6]Leidos Inc., Reston, VA, USA

Key Points:

- Fusion of multiple remote sensing estimates is a promising approach to generate high resolution daily estimates of snow cover
- A new machine learning approach outperforms a state-of-the-art competitor
- Spatially-varying fitted random forests allow for geographically-distributed feature importance

Correspondence to:

S. Mahanthege,
srm6ky@umsystem.edu

Citation:

Mahanthege, S., Kleiber, W., Rittger, K., Rajagopalan, B., Brodzik, M. J., & Bair, E. (2024). A spatially-distributed machine learning approach for fractional snow covered area estimation. *Water Resources Research*, *60*, e2023WR036162. https://doi.org/10.1029/2023WR036162

Received 5 SEP 2023
Accepted 20 OCT 2024

Abstract Snowpack in mountainous areas often provides water storage for summer and fall, especially in the Western United States. In situ observations of snow properties in mountainous terrain are limited by cost and effort, impacting both temporal and spatial sampling, while remote sensing estimates provide more complete spacetime coverage. Spatial estimates of fractional snow covered area (fSCA) at 30m are available every 16 days from the series of multispectral scanning instruments on Landsat platforms. Daily estimates at 463m spatial resolution are also available from the Moderate Resolution Imaging Spectroradiometer (MODIS) instrument on the Terra satellite. Fusing Landsat and MODIS fSCA images creates high resolution daily spatial estimates of fSCA that are needed for various uses: to support scientists and managers interested in energy and water budgets for water resources and to understand the movement of animals in a changing climate. Here, we propose a new machine learning approach conditioned on MODIS fSCA, as well as a set of physiographic features, and fit to Landsat fSCA over a portion of the Sierra Nevada USA. The predictions are daily 30m fSCA. The approach relies on two stages of spatially-varying models. The first classifies fSCA into three categories and the second yields estimates within (0, 100) percent fSCA. Separate models are applied and fitted within sub-regions of the study domain. Compared with a recently-published machine learning model (Rittger, Krock, et al., 2021), this approach uses spatially local (rather than global) random forests, and improves the classification error of fSCA by 16%, and fractionally-covered pixel estimates by 18%.

1. Introduction

Snow cover estimates are essential in planning of water supply to anticipate flooding or drought conditions (Martinec, 1975). It is estimated that one sixth of the world's population depends on snow and ice melt for their water supply (Hock et al., 2006). Satellite imagery has become an important component of snow water equivalent estimation (Frei et al., 2012), but satellites differ in spatial and temporal coverage, making it difficult to utilize imagery from multiple sensors. For a given location, MODIS (Moderate Resolution Imaging Spectroradiometer) images from the Terra satellite are available daily at 463 m resolution. Comparatively, TM (Thematic Mapper) images from Landsat 5 and ETM+ (Enhanced Thematic Mapper Plus) images from Landsat 7 at 30 m are available from each sensor, but only every 16 days for a given location. In principle, Landsat snow cover estimates can be utilized to produce snow water equivalent estimates, but within the 16 days overpass time, snow can melt, accumulate, and melt again. The Landsat Sentinel Harmonized dataset (Claverie et al., 2018) provides coverage every 3.5 days on average over the Sierra Nevada USA (Bair et al., 2022). However, the combined sensor data are only available for more recent years while Landsat data is available for nearly 40 years. Future missions with a focus on hyperspectral data (Rast & Painter, 2019) with similar spatial resolutions to Landsat, like the Copernicus Hyperspectral Imaging Mission for the Environment, the German Aerospace Center's Environmental Mapping and Analysis Program, and the US NASA Surface Biology and Geology Mission (Turpie et al., 2023) may improve accuracy on days with observations, but do not provide daily coverage. Thus, there is a need to develop techniques that estimate snow properties at high resolution daily.

In this work we focus on fractional snow covered area (fSCA) from Terra MODIS and Landsat 5/7 TM/ETM+, which provide per-pixel percentage of area covered by snow at 463 and 30 m, respectively. Fractional

snow cover retrievals have used computationally simple methods like the Normalized Differences Snow Index (NDSI) which identifies snow based on brighter reflectances in the visible than shortwave infrared (Dozier, 1989). For example, this method is widely used and the basis for NASA's standard snow product MOD10 (Hall et al., 2002; Salomonson & Appel, 2004). These band ratio techniques do not explicitly account for the presence of mixed pixels that dominate even down to a few meters (Selkowitz et al., 2014). Newer approaches that utilize a physically based model and all available visible, near-infrared, and shortwave infrared wavelength satellite observations using spectral mixture approaches (Painter et al., 2009; Rittger, Bormann, et al., 2021) have been shown to produce more accurate estimates of snow cover (Aalstad et al., 2020; Masson et al., 2018; Rittger et al., 2013; Stillinger et al., 2023).

Currently, no satellite product can be used to produce daily fSCA with 30 m spatial resolution, hence several studies have focused on data fusion methods to downscale daily MODIS images to achieve comparable resolution to Landsat images. Berman et al. (2018) propose using a dynamic time warping algorithm to build a snow year curve from a target year and a query year. Another method used in Landsat and MODIS data fusion is the spatial and temporal adaptive reflectance fusion model (STARFM; Gao et al., 2006). Apart from the fSCA product, Landsat and MODIS data fusion have been applied to various remote sensing products such as land surface temperature (Hutengs & Vohland, 2016; Weng et al., 2014) and vegetation index products (Li et al., 2021). In Hutengs and Vohland (2016), the authors used a random forest to downscale land surface temperature from 1 km MODIS images to 250 m; the random forest approach was able to outperform a widely used algorithm for sharpening thermal imagery (TsHARP). Data fusion methods can be categorized into three avenues according to Hazaymeh and Hassan (2015): (a) models using spatial–temporal adaptive reflectance-fusion (STARFM), (b) unmixing data fusion models (U-STARFM), and (c) sparse representation based spatiotemporal reflectance fusion (SPSTFM) models. A detailed comparison of each method is given in Hazaymeh and Hassan (2015). While each method has pros and cons, a major barrier is the high computational expense given the large area covered in our study extent, discussed below. Also, some models are unable to perform well in heterogeneous land cover types (Hazaymeh & Hassan, 2015).

Several machine learning techniques have been used in fSCA estimation in past literature. Czyzowska-Wisniewski et al. (2015) and Dobreva and Klein (2011) use artificial neural networks (ANNs) for fSCA estimation in complex forested environments while Kuter (2021) implements random forests and support vector regression for fSCA from MODIS Terra data in European Alps and compares performance to that of ANNs and multivariate adaptive regression spline techniques. A significant problem with implementing such machine learning techniques is the increased volume of training data required when implementing them in a large and diverse study area over a long period of time. Luan et al. (2022) introduced an *m*-day dynamic strategy into the random forest training. However, as the authors point out, extending the aforementioned strategy to the global scope is challenging due to the increased training data volume; hence, the authors suggest training spatially local models independently, which is the main and novel focus of our proposed method in this paper.

Our objective is to spatially downscale daily MODIS fSCA images to the same resolution as Landsat. We focus on a study region that was explored previously in Rittger, Krock, et al. (2021), a subset of the Sierra Nevada USA. Rittger, Krock, et al. (2021) propose a two-stage machine learning approach to downscaling MODIS estimates of fSCA to the spatial resolution of Landsat. Conditioning on MODIS fSCA estimates and other physiographic features in the study area, the first stage in their model is a classification random forest that predicts whether a given pixel has zero snow, is entirely covered by snow, or is fractionally covered. The second stage uses a regression random forest to predict the amount of fractional snow cover for the latter class. We propose a generalization of the approach of Rittger, Krock, et al. (2021) that draws inspiration from a portion of the spatial statistics literature. In particular, we investigate the notion of locally-varying fitted models. The model of Rittger, Krock, et al. (2021) is fit using data from the entire study domain. We refer to this as a "global" approach in that all available data may be used for model training. We propose dividing the domain into sub-regions, and fitting model components separately within each sub-region, or window; this results in a "local" approach in that only geographically nearby data are used to train the model in a given sub-region. The main benefit of this approach is that nearby information tends to be most useful when predicting at a given location. Such an idea is not unusual in the remote sensing literature; other authors have

implemented a windowing concept to address the spatial variability of geographical features. For example, Wu et al. (2012) and Gevaert and García-Haro (2015) use a moving window centered at each pixel to identify similar neighboring pixels within the window. The authors assign feature weights based on spatial Euclidean distance before using such neighboring pixels in a prediction model focused on normalized difference vegetation index (NDVI). As far as we are aware, our proposal is the first localized machine learning algorithm for combining Landsat and MODIS estimates of fSCA.

The paper is organized as follows: Section 2 introduces the two-stage machine learning approach; Section 3 describes the data set and geographical information used in the study, while Section 4 discusses estimation. Section 5 contains results comparing our model to the global model of Rittger, Krock, et al. (2021) and Section 6 closes the paper with suggestions of future directions for research.

2. Proposed Downscaling Method

This section discusses a new machine learning approach for modeling fractional snow cover area (fSCA). We begin with a review of an extant approach, followed by our proposed generalization. Rittger, Krock, et al. (2021) propose a two-stage random forest model for downscaling daily estimates of fSCA from MODIS to the spatial resolution of Landsat. Let $Y(s,t) \in [0,100]$ represent fSCA (in percent) for a spatial location $s \in \mathcal{D}$ in the domain of interest, $\mathcal{D}$, on day t. The model is

$$Y(s,t) = \begin{cases} 0, & X(s,t) = \text{no snow} \\ f(s,t), & X(s,t) = \text{some snow} \\ 100, & X(s,t) = \text{full snow} \end{cases} \quad (1)$$

where $X(s,t)$ is a categorical variable determining whether $Y(s,t)$ falls into the classes of no snow (no snow), snow within (0, 100) percent (some snow), or a fully-covered snow pixel (full snow). Rittger, Krock, et al. (2021) modeled $X(s,t)$ as a classification random forest with features including the MODIS estimate of fSCA, as well as other physiographic and climatic variables. If $X(s,t) =$ some snow for a given location, Rittger, Krock et al. (2021) additionally modeled $f(s,t)$ as a regression random forest, conditioned on the MODIS estimate of fSCA, as well as other physiographic and climatic variables. The combination of the two random forests explains the "two stage" algorithm. In preliminary analyses, Rittger, Krock et al. (2021) found that the two stage approach produced superior estimates of fSCA over a single random forest model for the full distribution within [0,100]. Because the random forests are fit with data from the entire domain $\mathcal{D}$, we refer to the model of Rittger, Krock, et al. (2021) as a "global" model.

We propose generalizing the model of Rittger, Krock, et al. (2021) to allow for locally-adaptive models. In particular, suppose the study domain $\mathcal{D}$ can be represented as a disjoint union of subsets $\mathcal{D}_1, \ldots, \mathcal{D}_N$ such that $\bigcup_{d=1}^{N} \mathcal{D}_i = \mathcal{D}$. The proposed model is then

$$Y(s,t) = \begin{cases} 0, & X_d(s,t) = \text{no snow} \\ f_d(s,t), & X_d(s,t) = \text{some snow} \\ 100, & X_d(s,t) = \text{full snow} \end{cases} \quad (2)$$

where $d \in \{1,2,\ldots,N\}$. In the proposed model (2), we follow Rittger, Krock, et al. (2021) by modeling $\{X_d(s,t)\}$ as classification random forests, and $\{f_d(s,t)\}$ as regression random forests, but critically we only use data from $\mathcal{D}_i$ to train the model for $X_i(s,t)$ and $f_i(s,t)$. At any given point in the domain, our model is still a two-stage random forest approach, but the behavior of the random forests are allowed to change over the domain; we refer to the proposed model as a "local" model to distinguish it from (1).

This idea of locally-varying random forests warrants some further discussion. In the spatial statistics literature, the notion of spatially-varying models has been around for many decades; for example, Haas (1990) used a moving window to locally estimate a spatial model that was used for spatial prediction. In our setup we are not directly

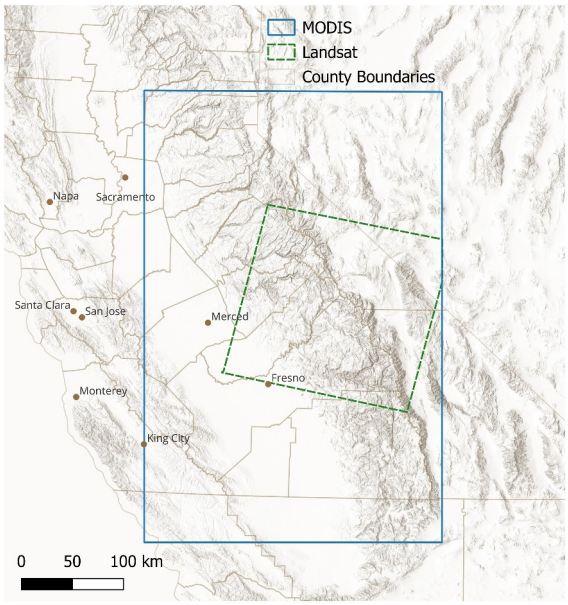

Figure 1. MODIS and Landsat study extent in the southern Sierra Nevada region.

concerned with spatial prediction, but rather allowing the model to adapt to (potential) locally-varying relationships between features and the response. Other authors (Gelfand et al., 2003) use a single regression-based model, but allow the coefficients to vary over space; our approach uses more powerful machine learning models, but incorporates the notion of local variation.

In a global model (1), the component random forests are trained using data from the entire domain. If geographic coordinates are included as a feature (e.g., latitude and longitude), then in principle the tree-based nature of a global random forest would allow it to adapt to the same spatially-varying characteristics as a local random forest. However, in our testing (see the results section), the local forest implementation substantially outperforms the global fit.

3. Fractional Snow Cover Area Data

To illustrate our approach, we focus on the same study area of Rittger, Krock, et al. (2021), located in the southern part of the Sierra Nevada mountain range, covering about 17,375 square miles (45,000 square kilometers), accounting for about 10% of the state of California as shown in Figure 1. Elevation within this region varies from sea level to about 4,000 m above sea level. Low elevation land is covered in shrubs and forests while high elevation regions have rocky mountains (Homer et al., 2015). Snowfall in this region starts in late fall and ends in spring but at high elevations snow cover lasts into early summer or can last all year.

Our study used data from Landsat 5 TM (Thematic Mapper) and Landsat 7 ETM+ (Enhanced Thematic Mapper Plus) instruments. Throughout we will refer to the estimates of fSCA from sensors flown on Landsat platforms simply as Landsat. Additionally we used data from MODIS Terra, which we will simply refer to as MODIS. Figure 2 shows an example day of the fractional snow cover area (fSCA) estimates from Landsat and MODIS on 18 February 2009 in the Sierra Nevada. Landsat shows finer spatial variation whereas the coarser

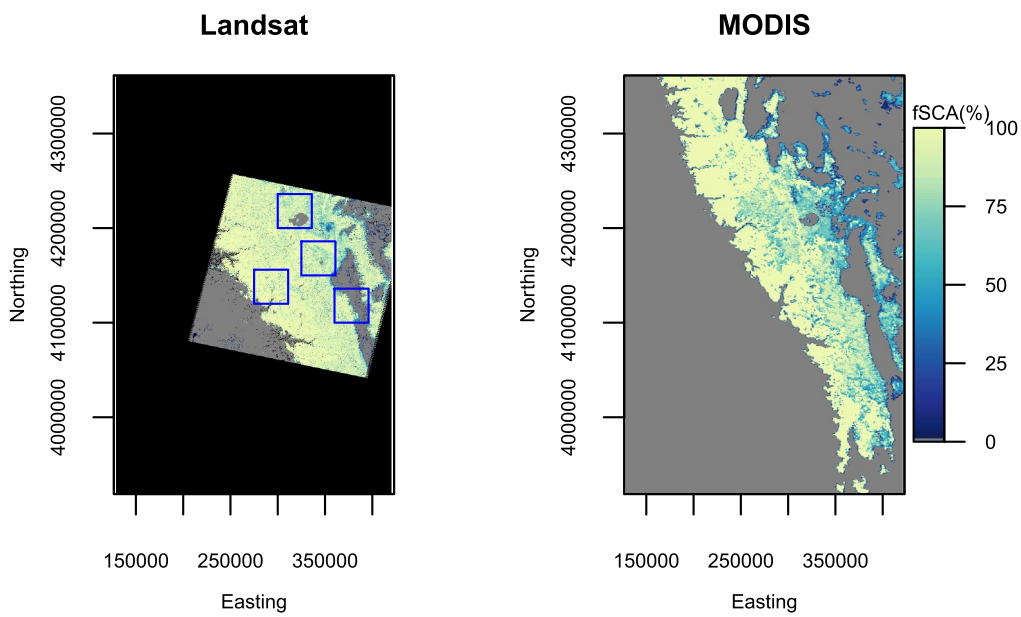

Figure 2. Fractional snow cover percentage (fSCA) from Landsat and MODIS on 18 Feb 2009 over a portion of the southern Sierra Nevada mountains. 0% fSCA appears as gray and missing data are shown in black. Sub-regions selected for model training are indicated by blue squares.

resolution of MODIS tends to smooth out fine scale variation. We apply spectral mixture analysis, specifically the Snow Covered Area and Grain Size (SCAG) model (Painter et al., 2003, 2009) to Landsat data. For MODIS we use spatially and temporally complete (STC) fSCA derived from the MODIS based SCAG implementation, MODSCAG. MODIS fSCA is available daily while Landsat fSCA is available every 16 days. We use the same subset of days from 2000 to 2011 for which pairs of MODIS and Landsat data are available and used in Rittger, Krock, et al. (2021). From this period, 167 days are obtained that approximately equally sample the different seasons within a year. Satellite images often are affected by cloud cover which makes part or the entire image unusable on certain days. For Landsat, areas affected by cloud cover on a given day are manually removed from the analysis. We used Landsat 5 and 7 scenes with up to 35% cloudiness. This initial training dataset biased Landsat observations to non-winter months. After visual inspection, some of these were removed, while many of them were hand-masked to remove clouds, resulting in the final set of data used. This approach allowed for better training data by both including a balanced number of Landsat data across months (days of the year) and excluding the use of automated cloud discrimination on single images, which typically have both errors of commission and omission. Clouds were masked by hand using RGB composites in which snow appears cyan and clouds white. In addition to the differences in color, the texture of the image allows one to discriminate snow from clouds. A gap-filling and smoothing technique was used to automatically discriminate cloud cover in MODIS images, which is fully described in previous literature (Rittger et al., 2020). Geographical features such as elevation, slope, aspect, average windspeed, barrier distances (from the northwest, southwest and west), and pixel distance to the ocean in the southwest and west directions are considered as covariates based on their fSCA predictive ability highlighted in Bair et al. (2016, 2018) and Fassnacht et al. (2012). In particular, the selected features are the same as in Rittger, Krock, et al. (2021). Elevation (height above sea level) ranges from sea level to approximately 4,000 m within our study area. Slope in degrees is computed using the digital elevation map. Aspect ranges from -1 to 360°, with -1 given for flat areas. Average windspeed ranges from 0 to 24 m/s. Barrier distances from northwest, southwest and west directions (nw. barrierdist, sw. barrierdist, and w. barrierdist, respectively) are the elevation differences between a given pixel and the highest pixel in a particular direction, in meters. Finally, pixel distances to the ocean in the southwest and west directions (sw. waterdist and w. waterdist, respectively) are used to account for the distance to the Pacific Ocean, where winter storms originate. These features have a high spatial variation within our study area, hence, we anticipate that incorporating geographical features in the model may account for some local variation in fSCA that daily MODIS is unable to provide. In addition to these physiographic features and MODIS, we include a day of year predictor similar to Rittger, Krock, et al. (2021).

4. Estimation

In this section we discuss the estimation approach for both the component classification and regression random forests. The local model additionally requires choice of the subdomains $\{\mathcal{D}_i\}_{i=1}^{N}$. Although training samples differ, both global and local models are fit using standard techniques for random forests.

4.1. Model Estimation

Random forests combine a number of decision trees in classification or regression problems (Breiman, 2001). Briefly, a random forest is generated by fitting different decision trees to training data. Individual trees are fit in a stepwise fashion by splitting the feature domain into hyperrectangles; the feature and value over which the split occurs is chosen to minimize a training statistic. Splitting is continued until a minimum node size is reached. The final forest predictor is created by combining the predictions from each component tree.

In both the global and local models, the first stage is to use a classification forest to classify fSCA into $K = 3$ factors (no snow, some snow or full snow). The split decision at node m is made based on minimizing the Gini index (G_m). Let N_m be the total number of data points at node m representing the feature region R_m and let $\hat{p}_{mk}$ be the empirical probability of class $k = 1, \ldots, K$ in the region R_m. That is, if there are n_k number of points of class k data in region R_m, then $\hat{p}_{mk} = n_k/N_m$. The Gini index value at node m is then

$$G_m = \sum_{k=1}^{K} \hat{p}_{mk}\left(1 - \hat{p}_{mk}\right) = 1 - \sum_{k=1}^{K} \hat{p}_{mk}{}^2. \tag{3}$$

The second stage is a regression forest component in both global and local models. The regression forest is fit in a similar fashion, but using mean squared error as the objective statistic.

In our implementation, we use the *ranger* package (Wright et al., 2020) in `R` to implement fast random forest algorithms with 100 trees and randomly choose from $\lfloor\sqrt{p}\rfloor$ number of variables as candidates to split at each node (Hastie et al., 2009), where $p = 11$ is the total number of predictors in both classification and regression forests. For a fair comparison of model performance between global and local approaches, model hyperparameters were kept consistent with Rittger, Krock, et al. (2021).

4.2. Sub-Region Choice

The global model uses data from the entire study domain $\mathcal{D}$, while the local model fits different random forests over each subdomain $\{\mathcal{D}_i\}_{i=1}^{N}$. In principle these subdomains can be of any shape, or can stratify the study domain in any way as long as they are disjoint. We opt to use regular squares for the shape of our subdomains, effectively splitting the study domain into uniform tiles or blocks; however, the choice of the size of these blocks remains a question.

Experimenting with different block sizes over the entire study extent is computationally expensive; thus we extracted four different $1,200 \times 1,200$ sub-regions from the study domain as shown in Figure 2 and sample block sizes within these sub-regions. These sub-regions were chosen to span reasonable variation over the available features, and sample different climatic zones from valleys to high alpine areas. To identify a block size and sample size choice for the local model, we fit different random forest models within each block, using training samples only within the block itself.

We define two statistical measures to compare classification model performance for testing and choosing sub-region size. Classification error (C_d) and probabilistic error (P_d) for a region d in the study extent are given in Equations 4 and 5 where N_d is the number of testing pixels in each sub-region (after removing data used in the training process) and $s \in \{1,\ldots,N_d\}$. These validation statistics are computed for each day t in our training set. Calling $\mathcal{D}_{dr}$ the testing data subset of sub-region $\mathcal{D}_d$, and letting $\hat{X}(s,t)$ denote a predicted value of snow class under a given model, classification error and probabilistic error are defined by

$$C_d = \frac{1}{N_d} \sum_{X(s,t)\in D_{dr}} I_{[X(s,t)\neq\hat{X}(s,t)]} \tag{4}$$

$$P_d = \frac{1}{N_d} \sum_{X(s,t)\in D_{dr}} \left(1 - \hat{P}(X(s,t))\right) \tag{5}$$

where I is the indicator function which takes value 1 when $X(s,t) \neq \hat{X}(s,t)$ and 0 otherwise, and $\hat{P}(X(s,t))$ is the predicted probability of the actual class.

Classification error can be seen to quantify the quality of the point predictions of {no snow, some snow, full snow} and takes values in [0,1] with 0 indicating perfect predictions, and one indicating no single prediction is correct. Probabilistic error also takes values in [0,1] and quantifies the quality of the confidence of the predictions and is negatively oriented.

For the local classification models, we vary block size from 150×150 pixels to 600×600 in increments of 50 pixels per side; that is, we increase the block size from blocks with an area of 20.25 km^2 up to blocks with an area of 324 km^2. Simultaneously, we vary sample percentage (number of pixels sampled over total pixels) from $25\% - 45\%$ in 5% increments; samples are drawn completely at random from the block under consideration. This training sample percentage represents the percentage of data for a given day to be used as part of the training data. For each training size and block size pair, we compute predictive classification and probabilistic errors for the testing data within that region; these statistics are then averaged across the four training regions. Figure 3 shows the averaged classification and probabilistic errors as a function of block and sample size. The most striking pattern is that, with a larger percentage of training samples, both types of error are reduced. However, perhaps

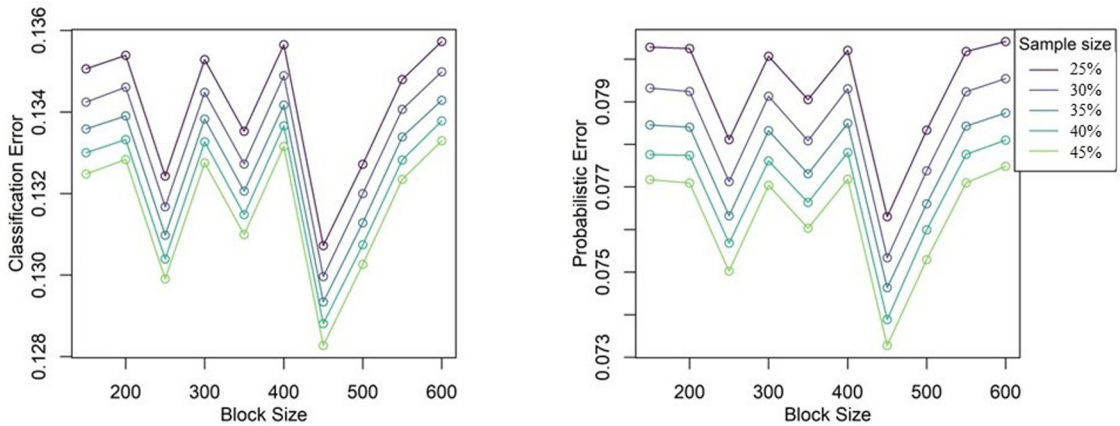

Figure 3. Classification and probabilistic error (averaged over four training regions) from the local classification random forest for different block sizes and different sample size percentages.

somewhat surprisingly, there is not a strong trend in prediction error over block size. In principle, extremely small blocks would have so little data that the model overfits, whereas extremely large blocks would "smear out" the local effects of the features. The minimum predictive error values are achieved when block size is 450 × 450 irrespective of the sampling size, and thus for the remainder of this work we use blocks of marginal dimension 450 for the local classification forests. Although there is clear evidence that larger training sample sizes reduce predictive errors, there is an additional trade off with the computational time required to fit the models; we thus opt for using 35% of available data to train the classification models, balancing between goodness-of-fit and predictive accuracy. Assuming complete data are available, this would yield approximately 71,000 training pixels per available day in each block. In practice, some blocks will have lower training sizes due to missing data. Appendix A shows each block's class percentage in the training dataset.

In the second stage of the model, we require a regression random forest to predict values of fSCA in (0, 100); we adopt a similar experimental setup to identify a block choice. In particular, we vary block size from 150 × 150 pixels to 1,000 × 1,000 in increments of 50 pixels per side for each of the four sub-regions, fit a regression random forest on half of available training data for a given block and record predictive accuracy on the remaining held-out testing data. The larger possible block size is due to the fact that fewer pixels have fSCA strictly within (0, 100), and thus potentially a larger block size is necessary to capture sufficient data to inform the model. If a given day has fewer than 100 available samples, it is removed from the training data. Note that we do not vary the sample size proportion as in the classification experiment—when training the classification model, any (non-missing) pixel can be used to train the model whereas for the regression model only pixels with fSCA strictly in (0, 100) can be used; this represents a substantial decrease in available training data overall. Figure 4 shows predictive root mean square errors averaged over the four sub-regions as a function of training block size. Similar to the classification block size study, there is not a strong trend

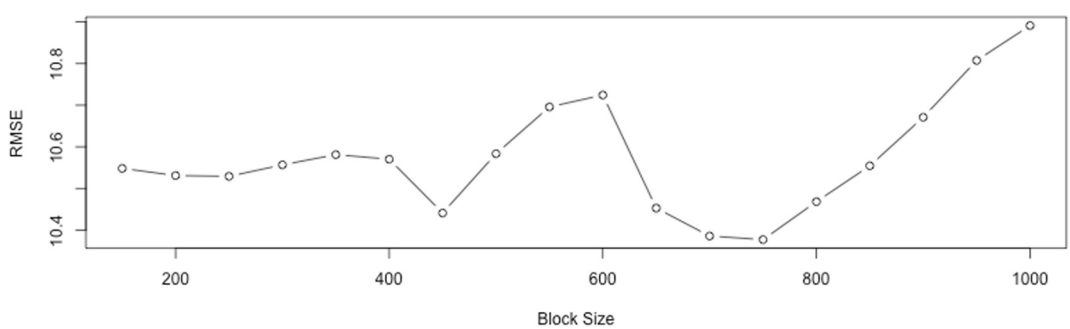

Figure 4. Root mean square error (averaged over four training regions) from the local regression random forest experiment for different block sizes. Values are percent fSCA.

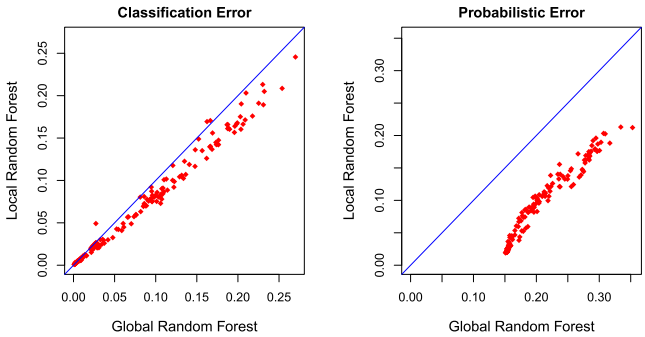

Figure 5. Daily average classification error and probabilistic error based on the local random forest and global random forest predictions on testing data.

across different block sizes, except an apparent degradation of performance at the largest block sizes. For the remainder of this work we adopt a 750 × 750 block size for the second stage of the local model.

Computations are performed on a University of Colorado Research Computing cluster node with 180 GB RAM and 64 Intel Skylake cores. For a given block D_i, local classification and regression forest each take approximately 30 min to fit. Predictions based on the local model for a given day take approximately 3 hours for the whole study domain.

5. Results

We fit both the global and local downscaling models to all 167 available days of data. As described in the prior section, subsets of the data are used to train the model; in this section validation statistics are reported for the held-out testing data on which the local forests were not trained. If a given day and region has insufficient data to train the local forest model, in practice we revert to the global model predictions; validation statistics below are given only for cases where the local model is available.

We begin with validation of the first stage classification models. Figure 5 shows validation statistics from the proposed local classification random forest method compared to the global random forest approach. Classification and probabilistic errors are computed on testing data over the entire study extent for each day. Figure 6 displays the same values but as a function of day of year. Keep in mind that, although plotted over day of year, each validation day comes from a (potentially) different year in the period 2000–2011. The November to May time period (days 1–150 and 300–356) shows the most variation in prediction between the two models as this is the time frame where new snow is deposited in the Sierra Nevada. During the summer months irrespective of the model used, fSCA is predicted with nearly 0% error as there is no snow cover on these days. However, the probabilistic error illustrates that the local model is substantially more confident in the most-likely class probabilities. Table 1 shows the classification and probabilistic errors averaged over 167 days for the entire study area. Average classification error is reduced from approximately 8.4% to 7.1% (a 16% improvement) while average probabilistic error is reduced from approximately 20% to 8.7% (a 57% improvement). Since there is a variation in prediction performance during summer months versus winter months, we see a high standard deviation in probabilistic and classification errors from both models. Together these results suggest there is substantial improvement using the local approach over the global approach for fSCA classification.

Sensitivity (percent of true positives) and specificity (percent of true negatives) are common additional measures of classification model goodness-of-fit. Figure 7 shows a time series of sensitivity and specificity for each class (zero percent snow, between zero and one hundred percent, and one hundred percent) with values computed for each day. Across the board it is clear that the local model has superior sensitivity and specificity compared to the global model, with particular improvement in the middle class across the year. The first row of graphs of sensitivity indicate that 0% snow cover category are mostly correctly predicted between both models, as sensitivity is close to one. However, summer and fall months from June to October have lower overall sensitivity in both the 0 – 100% class and 100% snow cover class due to the imbalance in snow

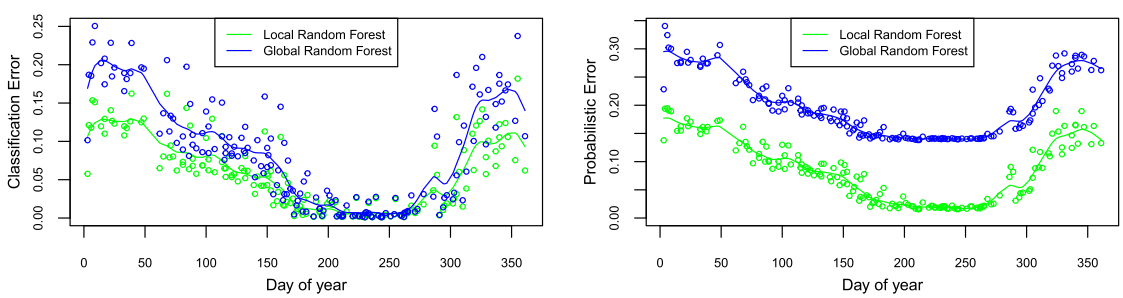

Figure 6. Same as Figure 5, by day of year. Classification error and probabilistic error shown as points with a spline smoother solid line.

Table 1
Average Classification and Probabilistic Error for Global and Local Models Along With Their Standard Deviation

	Classification error	Probabilistic error
Global Random Forest	0.0837 (0.0719)	0.2037 (0.0519)
Local Random Forest	0.0705 (0.0620)	0.0874 (0.0574)

classification frequencies during these months because the majority of the pixels have no snow. Even for these difficult cases, the local model has higher sensitivities compared to the global model. Similar results are reflected in the specificity graphs in the second row of Figure 7; during the summer months pixels that do not belong to the 0% snow cover category are incorrectly classified as 0% snow cover due to the imbalance in class frequencies during these months, while the local model mitigates this effect over the global model. During winter and spring months, sensitivity and specificity are both high for the boundary classes in both models. Appendix B shows the actual proportion of fSCA in each class for each day to better understand the class imbalance due to seasonality. Overall, the local model performs as well as, or better than, the global model across all seasons and class predictions. Next we consider the second stage of the model in predicting values within (0, 100).

We turn to validation of the second stage model that predicts values in the interval (0, 100) percent fSCA. In order to disentangle the predictive abilities of the classification and regression stages of the model, we only calculate error statistics conditionally on true values, predicted values from the global model, and predicted values from the local model being in (0, 100); otherwise some predictive improvement using the local model may simply be due to a better classification of being in class (0, 100) as opposed to a superior prediction of values within this class. Figure 8 shows the root mean squared error (RMSE) for predictions of values in (0, 100) for the local and global models' second stages, with a smoothing spline to show trends. Clearly there is substantial improvement across the year in predicting values within this class using the local model over the global model. On average, on the fSCA scale the RMSE is reduced by approximately 3%, relative to the global model this an approximate 18% improvement. Comparing Figures 7 and 8 we see that higher RMSEs reflect seasonal loss in sensitivity and specificity.

Next we consider a visual comparison of the downscaled fSCA images produced by the global and local models. Figure 9 shows estimated percentage fSCA for MODIS, the global model, the local model and the validating Landsat image for 18 February 2009. Four subregions are also included at higher resolution for ease of visual comparison. Subregions 1 and 2 contain Lakes Crowley and Mono, respectively, while subregions 3 and 4 contain the Upper San Joaquin River Basin and the Owens Valley, respectively. Subregions 3 and 4 illustrate two important aspects of the local model—there is generally better identification of regions of very high snow cover (i.e., 100% fSCA) using the local model than the global model, which tends to underpredict fSCA for high values, and the spatial coverage of the local model is generally more accurate. For example, in Subregion 3, the valley in which the MODIS retrievals show no snow is slightly filled-in using the global model, whereas the local model predicts high values of snow except at a very narrow center of the valley, which better agrees with the validating Landsat imagery than the global model. Subregion 4 shows finer details near the snow line (the boundary between regions with and without snow) using the local model than the global model, which tends to smear out values at this critical boundary. Although both models improve spatial resolution and accuracy over MODIS, the local model captures more accurate details in fSCA than the global model can produce. This claim is supported by quantitative statistics such as root mean squared error (RMSE) within each region—RMSE values for the global model in regions 1–4 are 14.7,

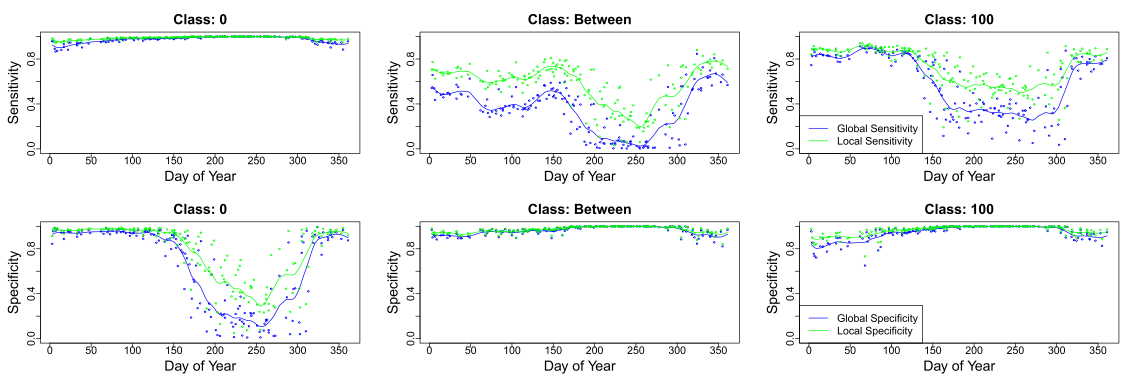

Figure 7. Model sensitivity and specificity for global random forest and local random forest approaches. Solid line is a smoothing spline while points show actual values.

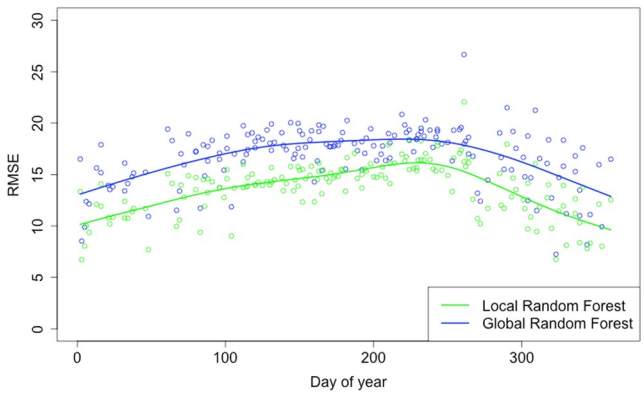

Figure 8. Root mean squared error (RMSE) for the second stage of the local and global models, predicting values in (0, 100) percent fSCA for the 167 available validation days; dots are values by day of year while the solid line is a spline smoother to aid the eye.

14.1, 26.0 and 20.4, respectively, while the local model has RMSE values of 10.6, 9.3, 12.7 and 13.3, respectively. Local predictions show improvement of RMSE between $27\% - 51\%$ over the global model in these four subregions.

We close this section with an investigation of feature importance in the component models. Due to the complex multi-tree nature of random forests, it is not straightforward to identify which features yield strong predictive power. Feature importance methods for ensembles of trees have been proposed, and typically focus on tracking the reduction in a statistic (e.g., the Gini index for classification, or mean squared error for regression) at each node in each component tree that is achieved when splitting over a particular feature. The reduction for a given feature is tracked across all nodes and trees, and is then aggregated into a single value which, when compared to the other features' aggregate reductions, can be interpreted as a quantification of that particular feature's relative importance (Hastie et al., 2009). In Rittger, Krock, et al. (2021), the global classification forest and global regression forest feature importances are noted with MODIS, day of year and elevation capturing the main three contributions to improved Gini index and variance reduction, respectively. For the local model proposed in this work, it is not straightforward to generalize this notion of feature importance to a global domain. Indeed, with multiple random forests being spatially distributed over the domain, we instead propose a visual assessment of variable importances that allows us to track the relative importance of a given covariate over the study domain. We follow Rittger, Krock, et al. (2021) in using the improvement in Gini index, and reduction in variance, to quantify variable importances for the classification and regression stages of the model, respectively.

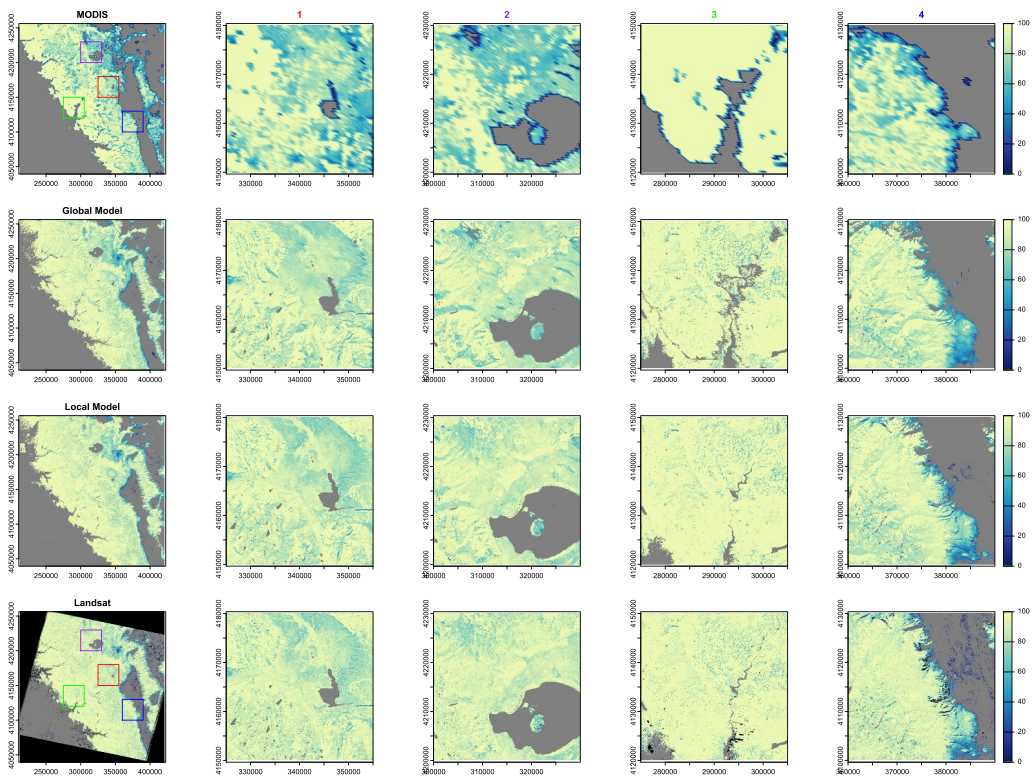

Figure 9. Percentage fSCA based on MODIS, the global model, the local model and validating Landsat for 18 Feb 2009. Black values indicate missing pixels. Four zoomed-in subregions are indicated by squares colored red (1), purple (2), green (3) and blue (4).

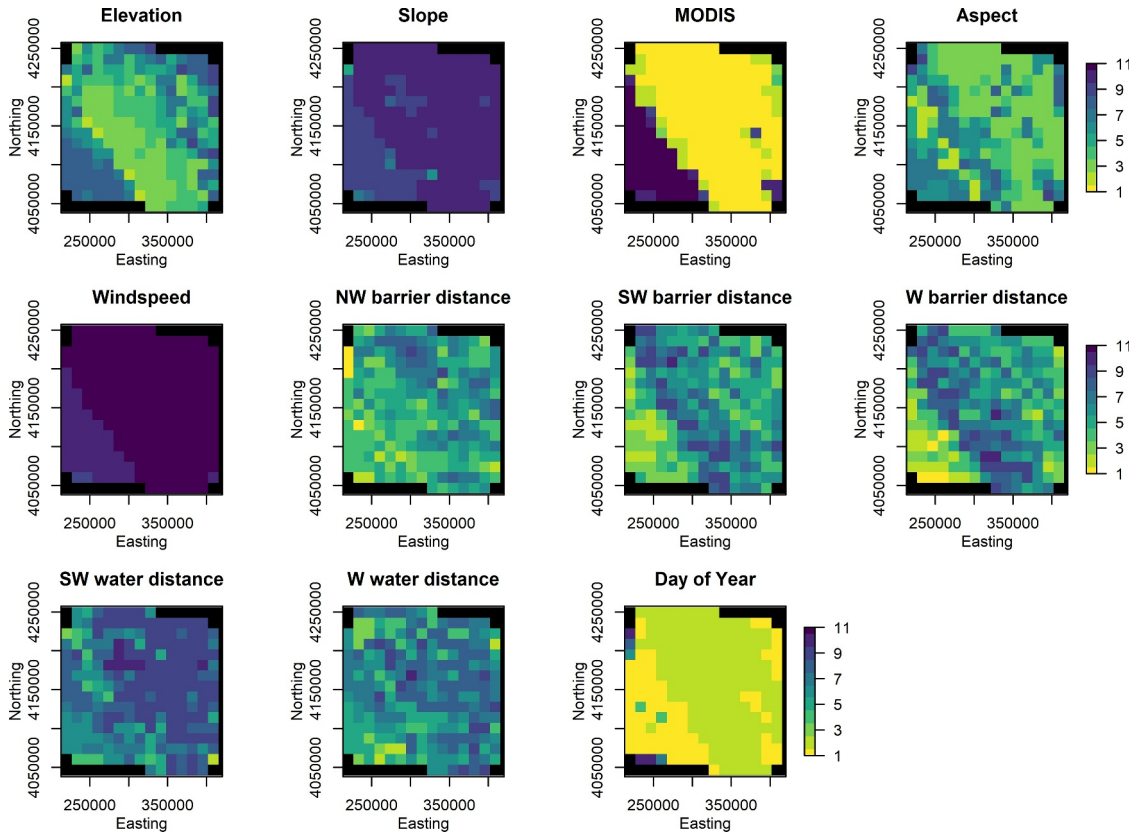

Figure 10. Rank of variable importance from most important (1) to least important (11) for the first stage classification models.

Figures 10 and 11 show the spatial distribution of the rank of each variable's importance over the study domain. That is, each sub-region has a fitted random forest with 11 features; the value displayed for any given sub-region in Figures 10 and 11 is the rank of a given variable for that particular sub-region, ordered from most important (rank 1) to least important (rank 11). A few comments are in order: first, the number of blocks is different between these two figures as the block sizes differ for each stage of the model. Second, there are more missing values for the second stage of the model than the first; this is due to the fact that there are fewer values of percentage fSCA in (0, 100) to allow for training in some sub-regions within the domain. Some interesting patterns emerge: MODIS holds the highest predictive value over nearly the entire domain for both stages of the model; however, at low elevations (i.e., the southwest corner of the domain), MODIS is not as useful for predicting fSCA class. This is sensible, however, as this valley rarely has snow, in which case the day of year is more predictive. Day of year is generally the second most important variable throughout the domain, followed by elevation and aspect. Elevation is generally most important in areas where there is substantial elevation variation, that is, in the mountainous terrain through the center of the domain. An interesting pattern emerges for aspect, where aspects on the southwest boundary of the mountain range tend to be more important than those just within the mountain range, perhaps due to the upslope precipitation effect. Various barrier distances, particularly those measuring distance to the west or southwest, tend to have higher importance at low elevations in the valley.

6. Discussion and Conclusions

In this study we introduce a new machine learning method for downscaling low resolution spatial estimates of fSCA to a higher resolution. The basic idea relies on segmenting the study domain into disjoint regions, over each of which a machine learning model is fitted. These segmented models can then downscale low resolution

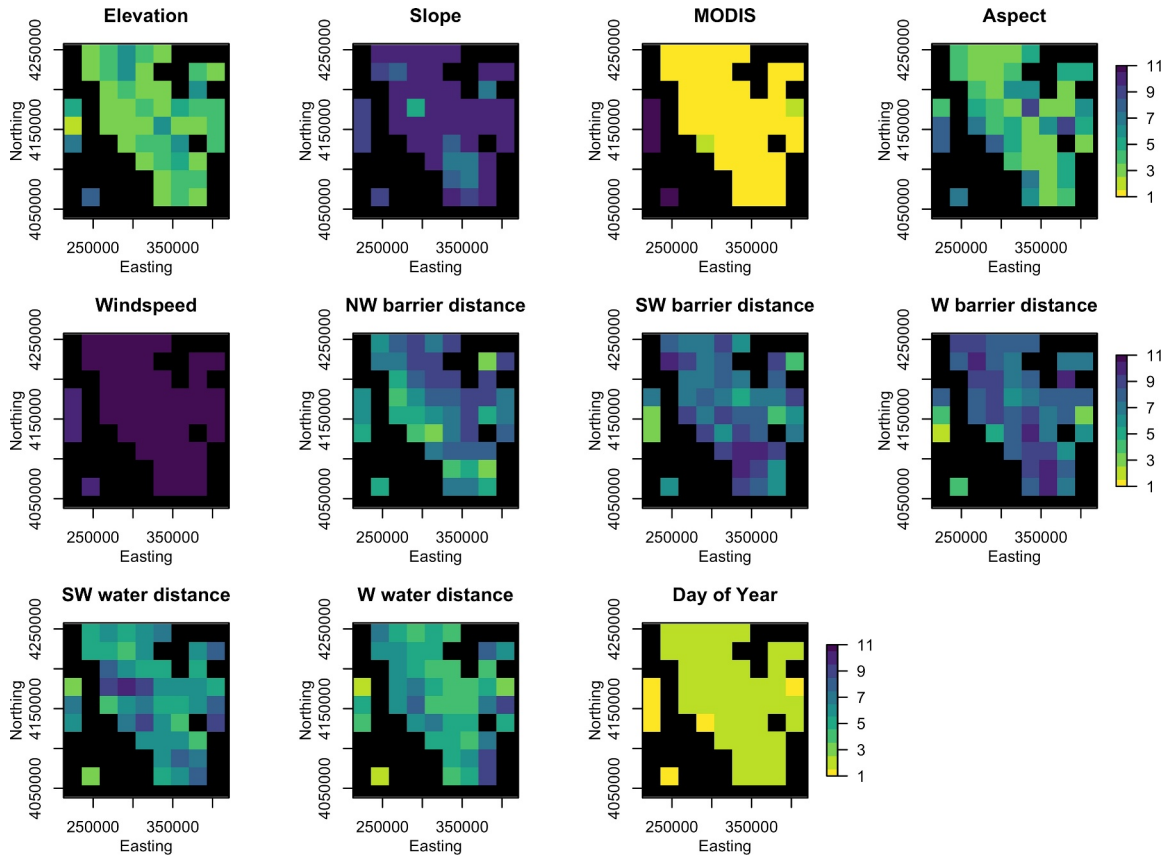

Figure 11. Rank of variable importance from most important (1) to least important (11) for the second stage regression models. Note the resolution is coarser than in Figure 10 due to the coarser gridding of the regression stage.

estimates of fSCA locally, allowing the fitted models to better adapt to local characteristics than a model fit over the entire study domain.

We apply the proposed model to downscaling fSCA to the 30 m resolution of Landsat using 500 m MODIS images and physiographic features as model features over a subset of the Southern Sierra Nevada mountain chain. We compare to the machine learning model of Rittger, Krock, et al. (2021), which is fitted globally—or over the entire spatial domain, on testing data and find that our proposed local model performs better across the entire distribution of fSCA. Variable importance measures for the local model indicate that significance of each feature varies spatially in our study area; such a detailed assessment of features is not straightforward to extract from a globally fitted ensemble model like the two stage random forest of Rittger, Krock, et al. (2021). Visual assessments indicate that applying this segmented technique does not lead to artificial edges between sub-regions in our study (not shown).

In a companion work we compared the first classification stage of our model to a set of competing statistical models (Mahanthege, 2021). In particular, in each domain localized multinomial logistic regression with and without regularization were fit and then compared against the proposed model. Neither statistical approach performed better than the proposed localized model, and sometimes performed worse than the global model of Rittger, Krock, et al. (2021); such results echo those of Rittger, Krock, et al. (2021) who also compared global logistic regression models to the machine learning approach.

There are many routes for future research based on our results. Although the current approach captures uncertainty in the class distributions, a comprehensive assessment of uncertainty for mixed cases would be an interesting and fruitful research direction. For example, one way to address the input uncertainty is to sample from the "prior" distribution of inputs and downscale them under the fitted model; this then would yield an ensemble of downscaled predictions that could be interpreted as samples from a predictive distribution. However, proper and robust uncertainty quantification for highly non-Gaussian variables like fSCA remains challenging, beckoning further statistical learning research. Alternatively, different distributed machine learning models may be explored. Extensions explicitly building in space-time information may be useful, perhaps tracking recent weather events when considering downscaling for a particular date. Although we utilize spatially-distributed sub-regions, another idea would be to generalize this approach to other features, perhaps fitting different models along elevation bands, or for different slopes and aspects. Finally, scaling up an approach such as the proposed to a large domain such as the CONUS is worth considering—the disjoint nature of the model allows for parallel computation, although experimenting with differing window sizes may be computationally prohibitive, depending on the domain size. In this work we use a set of physiographic and other feature variables that are sensible for the Sierra Nevada range; throughout a domain such as the CONUS we may expect other predictors to be useful, and certainly there is much room for considering geophysical model output (e.g., numerical weather prediction or reanalysis products) that will likely be helpful over such a heterogeneous domain. A final note is that over a large domain, we would expect the proposed locally-varying model to be substantially better than the global model of Rittger, Krock, et al. (2021) due to spatial heterogeneity.

Appendix A: fSCA Class Percentages in the Training DataSet

In the classification stage, we randomly sampled 35% of available pixels per day from each block to train each local forest. In Figure A1, we show the percentage of fSCA classes selected to train each block, which was computed by first summing the number of pixels belonging to each class for all days and dividing by the total number of training pixels. This gives the distribution of classes used in the training process which is important to highlight the class imbalance in different blocks. The southwest corner of the domain, which is the valley, rarely sees snow for most days; hence, we see a very high percentage of class 0 in the training dataset for blocks within that region. However, in the mountainous region, all three classes were sampled for most blocks.

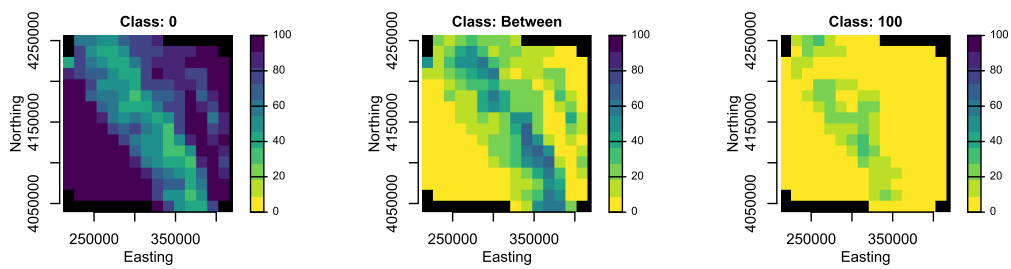

Figure A1. Training dataset fSCA class percentage for each trained block.

Appendix B: Actual fSCA Class Proportions for Each Day

Figure B1 shows the actual proportion of fSCA classes within the study region for each day in our validation dataset. On summer days, almost 100% of the data belongs to class 0, while all three classes are present in winter.

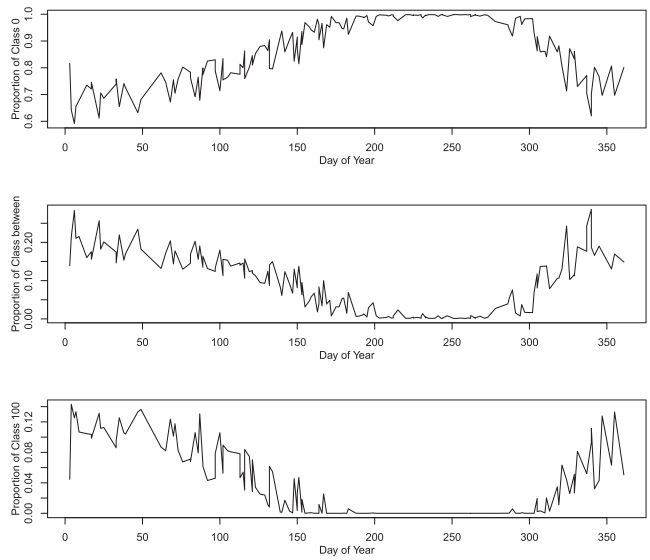

Figure B1. Actual fSCA class proportions for each validation day.

Data Availability Statement

To satisfy NASA open data policies, all data are available in online repositories in GEOTIFF format from Landsat and MODIS snow cover, predictors from Table 1, and snow cover from the 2-stage random forest model (Rittger, Bormann, et al., 2021). The 2-stage random forest model is currently on a public repository in GitHub at https://github.com/ShalMiz/SierraBighorn.

Acknowledgments
This work was supported by NASA grants 80NSSC24K1270, 80NSSC22K0929, 80NSSC22K0703, 80NSSC22K0686, 80NSSC20K1722, 80NSSC20K1349, and 80NSSC18K1489. Other support is from NSF DMS-1923062 and DMS-2310487. Computational tasks utilized the Blanca condo computing resource at the University of Colorado Boulder. Blanca is jointly funded by computing users and the University of Colorado Boulder.

References

Aalstad, K., Westermann, S., & Bertino, L. (2020). Evaluating satellite retrieved fractional snow-covered area at a high-arctic site using terrestrial photography. *Remote Sensing of Environment*, *239*, 111618. https://doi.org/10.1016/j.rse.2019.111618

Bair, E. H., Abreu Calfa, A., Rittger, K., & Dozier, J. (2018). Using machine learning for real-time estimates of snow water equivalent in the watersheds of Afghanistan. *The Cryosphere*, *12*(5), 1579–1594. https://doi.org/10.5194/tc-12-1579-2018

Bair, E. H., Dozier, J., Rittger, K., Stillinger, T., Kleiber, W., & Davis, R. E. (2022). Does higher spatial resolution improve snow estimates? *The Cryosphere Discussions*, *2022*, 1–20. https://doi.org/10.5194/tc-2022-230

Bair, E. H., Rittger, K., Davis, R. E., Painter, T. H., & Dozier, J. (2016). Validating reconstruction of snow water equivalent in California's Sierra n Evada using measurements from the NASA airbornes now observatory. *Water Resources Research*, *52*(11), 8437–8460. https://doi.org/10.1002/2016WR018704

Berman, E. E., Bolton, D. K., Coops, N. C., Mityok, Z. K., Stenhouse, G. B., & Moore, R. D. (2018). Daily estimates of landsat fractional snow cover driven by MODIS and dynamic time-warping. *Remote Sensing of Environment*, *216*, 635–646. https://doi.org/10.1016/j.rse.2018.07.029

Breiman, L. (2001). Random forests. *Machine Learning*, *45*(1), 5–32. https://doi.org/10.1023/A:1010933404324

Claverie, M., Ju, J., Masek, J. G., Dungan, J. L., Vermote, E. F., Roger, J.-C., et al. (2018). The harmonized landsat and sentinel-2 surface reflectance data set. *Remote Sensing of Environment*, *219*, 145–161. https://doi.org/10.1016/j.rse.2018.09.002

Czyzowska-Wisniewski, E. H., Van Leeuwen, W. J., Hirschboeck, K. K., Marsh, S. E., & Wisniewski, W. T. (2015). Fractional snow cover estimation in complex alpine-forested environments using an artificial neural network. *Remote Sensing of Environment*, *156*, 403–417. https://doi.org/10.1016/j.rse.2014.09.026

Dobreva, I. D., & Klein, A. G. (2011). Fractional snow cover mapping through artificial neural network analysis of modis surface reflectance. *Remote Sensing of Environment*, *115*(12), 3355–3366. https://doi.org/10.1016/j.rse.2011.07.018

Dozier, J. (1989). Spectral signature of alpine snow cover from the landsat thematic mapper. *Remote Sensing of environment*, *28*, 9–22. https://doi.org/10.1016/0034-4257(89)90101-6

Fassnacht, S., Dressler, K., Hultstrand, D., Bales, R., & Patterson, G. (2012). Temporal inconsistencies in coarse-scale snow water equivalent patterns: Colorado River Basin snow telemetry-topography regressions. *Pirineos: Revista de Ecología de Montaña*, *167*(0), 165–185. https://doi.org/10.3989/Pirineos.2012.167008

Frei, A., Tedesco, M., Lee, S., Foster, J., Hall, D. K., Kelly, R., & Robinson, D. A. (2012). A review of global satellite-derived snow products. *Advances in Space Research*, *50*(8), 1007–1029. https://doi.org/10.1016/j.asr.2011.12.021

Gao, F., Masek, J., Schwaller, M., & Hall, F. (2006). On the blending of the landsat and modis surface reflectance: Predicting daily landsat surface reflectance. *IEEE Transactions on Geoscience and Remote Sensing*, *44*(8), 2207–2218. https://doi.org/10.1109/TGRS.2006.872081

Gelfand, A. E., Kim, H. J., Sirmans, C. F., & Banerjee, S. (2003). Spatial modeling with spatially varying coefficient processes. *Journal of the American Statistical Association*, *98*(462), 387–396. https://doi.org/10.1198/016214503000170

Gevaert, C. M., & García-Haro, F. J. (2015). A comparison of starfm and an unmixing-based algorithm for landsat and modis data fusion. *Remote Sensing of Environment*, *156*, 34–44. https://doi.org/10.1016/j.rse.2014.09.012

Haas, T. C. (1990). Lognormal and moving window methods of estimating acid deposition. *Journal of the American Statistical Association*, *85*(412), 950–963. https://doi.org/10.2307/2289592

Hall, D. K., Riggs, G. A., Salomonson, V. V., DiGirolamo, N. E., & Bayr, K. J. (2002). Modis snow-cover products. *Remote Sensing of Environment*, *83*(1–2), 181–194. https://doi.org/10.1016/S0034-4257(02)00095-0

Hastie, T., Tibshirani, R., & Friedman, J. (2009). *The elements of statistical learning: Data mining, inference, and prediction*. Springer Science & Business Media. https://doi.org/10.1007/978-0-387-21606-5

Hazaymeh, K., & Hassan, Q. K. (2015). Spatiotemporal image-fusion model for enhancing the temporal resolution of landsat-8 surface reflectance images using modis images. *Journal of Applied Remote Sensing*, *9*(1), 096095. https://doi.org/10.1117/1.JRS.9.096095

Hock, R., Rees, G., Williams, M. W., & Ramirez, E. (2006). Contribution from glaciers and snow cover to runoff from mountains in different climates. *Hydrological Processes*, *20*(10), 2089–2090. https://doi.org/10.1002/hyp.6206

Homer, C., Dewitz, J., Yang, L., Jin, S., Danielson, P., Xian, G., et al. (2015). Completion of the 2011 national land cover database for the conterminous United States–representing a decade of land cover change information. *Photogrammetric Engineering & Remote Sensing*, *81*(5), 345–354.

Hutengs, C., & Vohland, M. (2016). Downscaling land surface temperatures at regional scales with random forest regression. *Remote Sensing of Environment*, *178*, 127–141. https://doi.org/10.1016/j.rse.2016.03.006

Kuter, S. (2021). Completing the machine learning saga in fractional snow cover estimation from modis terra reflectance data: Random forests versus support vector regression. *Remote Sensing of Environment*, *255*, 112294. https://doi.org/10.1016/j.rse.2021.112294

Li, R., Xu, M., Chen, Z., Gao, B., Cai, J., Shen, F., et al. (2021). Phenology-based classification of crop species and rotation types using fused modis and landsat data: The comparison of a random-forest-based model and a decision-rule-based model. *Soil and Tillage Research*, *206*, 104838. https://doi.org/10.1016/j.still.2020.104838

Luan, W., Zhang, X., Xiao, P., Wang, H., & Chen, S. (2022). Binary and fractional modis snow cover mapping boosted by machine learning and big landsat data. *IEEE Transactions on Geoscience and Remote Sensing*, *60*, 1–14. https://doi.org/10.1109/TGRS.2022.3198508

Mahanthege, S. (2021). *Modeling fractional snow cover area using locally varying spatial models (Master's thesis*. University of Colorado Boulder). Retrieved from https://www.proquest.com/openview/9c29e6721a4151f15faf2afeae6f7e53/1?pq-origsite=gscholar&cbl=18750&diss=y

Martinec, J. (1975). Snowmelt-runoff model for stream flow forecasts. *Hydrology Research*, *6*(3), 145–154. https://doi.org/10.2166/nh.1975.0010

Masson, T., Dumont, M., Mura, M. D., Sirguey, P., Gascoin, S., Dedieu, J.-P., & Chanussot, J. (2018). An assessment of existing methodologies to retrieve snow cover fraction from modis data. *Remote Sensing*, *10*(4), 619. https://doi.org/10.3390/rs10040619

Painter, T. H., Dozier, J., Roberts, D. A., Davis, R. E., & Green, R. O. (2003). Retrieval of subpixel snow-covered area and grain size from imaging spectrometer data. *Remote Sensing of Environment*, *85*(1), 64–77. https://doi.org/10.1016/S0034-4257(02)00187-6

Painter, T. H., Rittger, K., McKenzie, C., Slaughter, P., Davis, R. E., & Dozier, J. (2009). Retrieval of subpixel snow covered area, grain size, and albedo from modis. *Remote Sensing of Environment*, *113*(4), 868–879. https://doi.org/10.1016/j.rse.2009.01.001

Rast, M., & Painter, T. H. (2019). Earth observation imaging spectroscopy for terrestrial systems: An overview of its history, techniques, and applications of its missions. *Surveys in Geophysics*, *40*(3), 303–331. https://doi.org/10.1007/s10712-019-09517-z

Rittger, K., Bormann, K., Bair, E., Dozier, J., & Painter, T. (2021a). Evaluation of viirs and modis snow cover fraction in high-mountain Asia using landsat 8 oli. *Frontiers in Remote Sensing*, *2*. https://doi.org/10.3389/frsen.2021.647154

Rittger, K., Dozier, J., Hill, A., Lutz, J., Painter, T., & Painter, T. H. (2020). Canopy adjustment and improved cloud detection for remotely sensed snow cover mapping. *Water Resources Research*, *56*(6), e2019WR024914. https://doi.org/10.1029/2019WR024914

Rittger, K., Krock, M., Kleiber, W., Bair, E. H., Brodzik, M. J., Stephenson, T. R., et al. (2021b). Multi-sensor fusion using random forests for daily fractional snow cover at 30 m. *Remote Sensing of Environment*, *264*, 112608. https://doi.org/10.1016/j.rse.2021.112608

Rittger, K., Painter, T. H., & Dozier, J. (2013). Assessment of methods for mapping snow cover from modis. *Advances in Water Resources*, *51*, 367–380. https://doi.org/10.1016/j.advwatres.2012.03.002

Salomonson, V. V., & Appel, I. (2004). Estimating fractional snow cover from modis using the normalized difference snow index. *Remote Sensing of environment*, *89*(3), 351–360. https://doi.org/10.1016/j.rse.2003.10.016

Selkowitz, D. J., Forster, R. R., & Caldwell, M. K. (2014). Prevalence of pure versus mixed snow cover pixels across spatial resolutions in alpine environments. *Remote Sensing*, *6*(12), 12478–12508. https://doi.org/10.3390/rs61212478

Stillinger, T., Rittger, K., Raleigh, M. S., Michell, A., Davis, R. E., & Bair, E. H. (2023). Landsat, modis, and viirs snow cover mapping algorithm performance as validated by airborne lidar datasets. *The Cryosphere*, *17*(2), 567–590. https://doi.org/10.5194/tc-17-567-2023

Turpie, K. R., Casey, K. A., Crawford, C. J., Guild, L. S., Kieffer, H., Lin, G., et al. (2023). Calibration and validation for the surface biology and geology (sbg) mission concept: Recommendations for a multi-sensor system for imaging spectroscopy and thermal imagery. *Journal of Geophysical Research: Biogeosciences*, *128*(9), e2023JG007452. https://doi.org/10.1029/2023JG007452

Weng, Q., Fu, P., & Gao, F. (2014). Generating daily land surface temperature at landsat resolution by fusing landsat and modis data. *Remote Sensing of environment*, *145*, 55–67. https://doi.org/10.1016/j.rse.2014.02.003

Wright, M. N., Wager, S., & Probst, P. (2020). Ranger: A fast implementation of random forests. *R package version 0.12*, 1.

Wu, M., Niu, Z., Wang, C., Wu, C., & Wang, L. (2012). Use of modis and landsat time series data to generate high-resolution temporal synthetic landsat data using a spatial and temporal reflectance fusion model. *Journal of Applied Remote Sensing*, *6*(1), 063507. https://doi.org/10.1117/1.JRS.6.063507